Research Article

Christoph Holst* and Heiner Kuhlmann

Aiming at self-calibration of terrestrial laser scanners using only one single object and one single scan

Abstract: When using terrestrial laser scanners for high quality analyses, calibrating the laser scanner is crucial due to unavoidable misconstruction of the instrument leading to systematic errors. Consequently, the development of calibration fields for laser scanner self-calibration is widespread in the literature. However, these calibration fields altogether suffer from the fact that the calibration parameters are estimated by analyzing the parameter differences of a limited number of substitute objects (targets or planes) scanned from different stations.
This study investigates the potential of self-calibrating a laser scanner by scanning one single object with one single scan. This concept is new since it uses the deviation of each sampling point to the scanned object for calibration. Its applicability rests upon the integration of model knowledge that is used to parameterize the scanned object.
Results show that this calibration approach is feasible leading to improved surface approximations. However, it makes great demands on the functional model of the calibration parameters, the stochastic model of the adjustment, the scanned object and the scanning geometry. Hence, to gain constant and physically interpretable calibration parameters, further improvement especially regarding functional and stochastic model is demanded.

Keywords: terrestrial laser scanner, systematic errors, self-calibration, calibration field, network configuration

DOI 10.1515/jag-2014-0017
Received August 08, 2014; accepted October 28, 2014.

***Corresponding Author: Christoph Holst:** Institute of Geodesy and Geoinformation, University of Bonn, Germany, E-mail: c.holst@igg.uni-bonn.de
Heiner Kuhlmann: Institute of Geodesy and Geoinformation, University of Bonn, Germany

1 Introduction

The use of terrestrial laser scanners (TLS) has become widespread in engineering geodesy since several years (e.g., [8, 14, 46]). Analyzing area-based deformations [18] as well as monitoring the growth of plants [34] are examples, where the high sampling density as well as upgrading point accuracies are the relevant aspects leading to the use of scanners. Simultaneously, the focus of interest has shifted in the recent past from only using the point cloud measured by the laser scanner to scrutinizing the point cloud as a result of the measurement process itself. This accompanies with the desire of operators and research institutions to understand and reproduce the measurement process of a laser scanner, e.g., similar to the one of a tacheometer. Unfortunately, this measurement process – being due to the specific construction of each laser scanner – is mostly hidden to the users and can only be regarded as a black box.

Additionally, – what might even be of greater significance – the processing of the raw measurements $\mathbf{l}_j = \left[s_j, \beta_j, t_j\right]^T$ (the polar coordinates distance s, vertical angle β and horizontal angle t of number $j = 1, \ldots, n$) resulting in the cartesian coordinates $\mathbf{x}_j$ does not have to be implemented straightforward by the manufacturers. This would mathematically equal

$$\mathbf{x}_j = \begin{bmatrix} x_j \\ y_j \\ z_j \end{bmatrix} = \begin{bmatrix} s_j \cdot \sin\beta_j \cdot \cos t_j \\ s_j \cdot \sin\beta_j \cdot \sin t_j \\ s_j \cdot \cos\beta_j \end{bmatrix} \tag{1}$$

in a right-handed trihedron [17]. However, even the polar coordinates s, β, t as well as the resulting cartesian coordinates x, y, z might be influenced by calibration parameters unknown to the user. Consequently, the user might only guess the preprocessing steps that have already affected the cartesian coordinates equaling the output of the instrumental-specific software after a measurement process.

Both aspects, i.e., the unknown measurement process due to the specific construction of a TLS as well as the unknown mathematical preprocessing, complicate the manageability of laser scanner measurements. Thus, the task of calibrating a TLS before using the point cloud for high accuracy analyses has become more crucial and important. This especially holds since the error budget of a TLS is no longer dominated by random errors but by the systematic errors that are to be calibrated.

This situation has resulted in many publications aiming at calibrating either single components of a TLS [7, 31, 44, 47] – e.g., also a radiometric calibration [19] – or the complete TLS as a closed system [29, 35, 36, 41]. Generally, calibrating a TLS considers two different aspects:

1. the construction of the TLS needs to be known – or, at least, it needs approximately to be known – to build up calibration parameters and
2. the calibration parameters need to be estimated by building up a qualified calibration field.

The first aspect is handled most times by assuming that the construction is similar to the one of a tacheometer [26, 27, 40]. This can be a first approximation of the construction regarding panoramic scanners with rotating mirrors. Thus, typical tacheometric systematic errors, e.g., horizontal collimation error, trunnion axis error or the zero error of the distance unit, equal the calibration parameters [1, 20, 21, 39]. For dealing with the second aspect, strategies for self-calibration developed in the recent years. Here, the scanner measurements themselves are used to analyze systematic deviations in the measurements and to relate them to the calibration parameters that are modeled.

The present study focuses on the second aspect of estimating the calibraton parameters by self-calibration; the first aspect of parameterizing the systematic TLS errors due to its construction is assumed to be given by previous studies. A new strategy for laser scanner self-calibration differing from all previous ones will be introduced and evaluated. It covers the central questions of this study:

Is it feasible to self-calibrate a TLS based upon one single scan of one single object? If yes, which requirements have to be met regarding the scanned object, the measurement geometry, functional and stochastic model?

This concept is new since it uses the deviations of each scanned point for calibration instead of some parameterized substitute objects as targets or planes. This will be explained in more detail in the following sections. After recapitulating typical calibration parameters assuming a panoramic TLS, the calibration procedure is simulated and analyzed. Finally, real measurements are used to calibrate the Leica Scan Station P20.

This new concept for laser scanner self-calibration only discovers instrumental errors – similarly to the already existing strategies. Other groups of errors, i.e., atmospheric based, geometry based and object based errors are not considered up to now. They need to be investigated additionally for a complete analysis of the TLS stochastic model [42, 46].

2 Strategies for laser scanner self-calibration

For laser scanner self-calibration, many studies exist. These are summarized in the following to distinguish the new, proposed strategy afterwards.

2.1 Previous studies

In previous studies that aim at laser scanner self-calibration, calibration fields are built up that help to separate the scanner specific systematic errors from sampled surfaces and objects. Therefore, objects are needed that can be parameterized. Until now, as objects either targets or small planes are used [2, 11, 12, 38] or boths objects are compared [3–5]. These targets or planes are placed in a calibration room of several meters size and they are scanned from varying stations and – if possible – in both faces. After calculation of each target's parameters (three-dimensional position) or each plane's parameters (normal vector and distance) from each station, these parameters of corresponding objects are related to each other by a coordinate transformation. Thus, the difference between the parameters of each object scanned at station 1 to the ones scanned at station 2 can be related to systematic errors of the TLS [10, 12, 29, 35, 38].

This procedure for laser scanner self-calibration is widespread. The quality of the estimated calibration parameters can directly be related to the network configuration of the adjustment. Here, the number of targets or planes, respectively, and their spatial arrangement are crucial. Both aspects lead to the magnitude of correlation between the estimated (calibration) parameters and to their accuracy being the most important quality measures for the calibration test field [28, 29]. Furthermore, the residuals after calibration are always analyzed regarding their

randomness and their decrease indicated by their standard deviation [37].

Consequential, using the existing strategies for laser scanner self-calibration rests methodically on parameterizing the differences of a spatial coordinate transformation based upon the parameters of targets or planes. Limiting aspects are the number of objects to be parameterized and the correlation and accuracy of the calibration parameters due to the network configuration.

2.2 Idea of the presented strategy

The calibration schemes recapitulated in the previous paragraph are very similar to calibration fields of tacheometers. Only one additional step is needed: the parameterization of discrete, selected objects out of the measurements. When calibrating a tacheometer, this step is obsolete since discrete, selected and signalized points can be measured (repeatedly and in two faces).

These previous calibration strategies do not profit from the individual information about the systematic TLS errors that is contained in the large amount of densely sampled points. Instead, the large number of points is reduced to several objects of limited number to estimate the calibration parameters. By this procedure, it is assumed that the systematic errors are constant on each object. The variation of the systematic errors inside this object – whose significance is due to the size of the object and its shape – gets lost in this step. It is only contained in the variance of the estimated object parameters, but its systematic trend is neglected. This situation is unsatisfying for laser scanner self-calibration.

Out of this observance, the present study explores the potential of using only one single scan from one single object for self-calibration. At this approach, the deviations of the measured points to this object are used themselves – and not the deviations between the parameters of several objects – to estimate the calibration parameters. On the one hand, this approach would benefit from the large number of observations used for calibration – since each observation contains individual information about the systematic TLS errors. On the other hand, it would suffer from a predetermined network configuration of the adjustment due to object geometry and scanning geometry.

Continuing this idea, systematic errors of a TLS can be detected simply by surface approximation when scanning an object that achieves special requirements: it needs to be very large so that it nearly covers the whole point cloud of a complete panoramic scan, its construction needs to be very accurate to distinguish the systematic errors from this object and the construction needs to be very simple. The last point ensures that the object can be parameterized with only few parameters and that no further influences, i.e., geometry and object based errors, disturb the analysis.

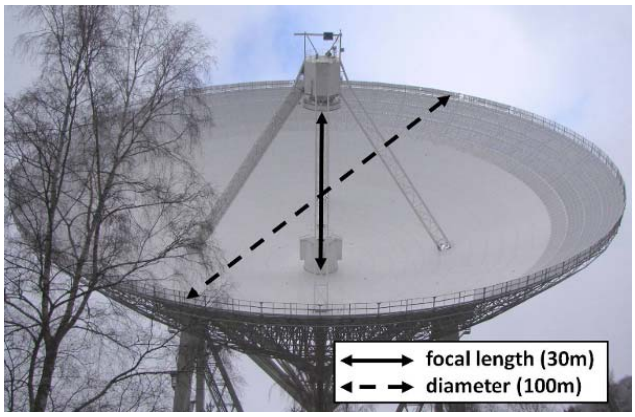

Fig. 1. Effelsberg radio telescope.

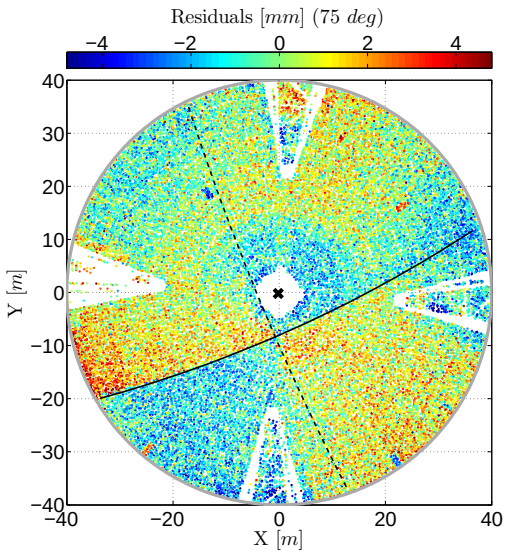

Fig. 2. Post-fit residuals after approximation of best-fit surface to laser scan at 75 *deg* elevation angle shown in object coordinate system $[X, Y, Z]$; transformation of TLS x-axis (lined), y-axis (dashed) and station (cross) in object coordinate system.

The main reflector of the Effelsberg radio telescope (Fig. 1) combines all mentioned aspects. Fig. 2 shows the residuals of an approximation representing the deviations between best-fit surface and laser scan. Since we can assume the main reflector to be more precisely constructed than the visible systematic residuals, they can be regarded to result from the systematic errors of the TLS.

The main reflector's diameter equals 100 m and its focal length f approximately 30 m; it can be parameterized

as a rotational paraboloid by

$$\frac{X_j^2 + Y_j^2}{4 \cdot f} - Z_j = 0 \tag{2}$$

where $[X, Y, Z]$ is the coordinate system describing the paraboloid in its normal position [16, 18]. Transforming this equation into the TLS coordinate system $[x, y, z]$, the transformation

$$\mathbf{X}_j = \begin{bmatrix} X_j \\ Y_j \\ Z_j \end{bmatrix} = \mathbf{R}_y(\varphi_y) \cdot \mathbf{R}_x(\varphi_x) \cdot \mathbf{x}_j + \mathbf{X}_v \tag{3}$$

is used where $\mathbf{R}_y(\varphi_y)$ and $\mathbf{R}_x(\varphi_x)$ equal the rotation matrices and $\mathbf{X}_v$ the translation vector. Consequently, the six parameters

$$\mathbf{p}_{\text{obj}} = [X_v, Y_v, Z_v, \varphi_x, \varphi_y, f]^T \tag{4}$$

are the ones to be estimated when parameterizing the main reflector measured by the TLS. Advantageoulsy, the focal length f is the only parameter describing the shape. By this parameterization as a rotational paraboloid using only the focal length f as shape parameter, model knowledge is integrated in the adjustment.

Now, the aim is to not only estimate the object parameters but also calibration parameters whose neglect causes the systematic residuals in Fig. 2. Similar to the existing strategies, the network configuration is crucial for this task. This network configuration only relies on one single station and the resulting measurement geometry this time. Nevertheless, previous studies showed that already the scanning of one object from one station builds up a network configuration that is worth investigating [13, 17].

3 Systematic errors of terrestrial laser scanners

For analyzing potential systematic errors of a TLS, the construction type needs to be investigated. The present study rests upon the Leica Scan Station P20 that approximately follows a tacheometric construction type with rotating mirror for beam deflection. The distances are measured by time-of-flight enhanced by the waveform digitizing technology [24].

Thus, calibration parameters for the distance unit as well as for the beam deflection can be assumed in the calibration model. However, these calibration parameters can be parameterized based on the TLS construction only approximatively and incompletely. This is due to the restrictive announcement of the constructurers regarding the scanners' constructions: as already stated, details are not known to the user [45].

3.1 Recapitulation of systematic errors

Systematic errors concerning the distance unit and the beam deflection are listed in several publications. However, due to the fact that the detailed construction is hidden from the user, the assumed parameters differ between the publications even though equal constructions are assumed. This is, amongst others, due to the fact that some studies only list the main error sources of tacheometers [39, 40] whereas some others explain all possible error sources leading to systematic deviations even if these are free of any physical interpretation [26, 30].

The present study only parameterizes the systematic errors related to the unavoidable physical misconstruction of the TLS; thus, only physically interpretable calibration parameters are assumed. These are modeled similar to a tacheometer. This tacheometric assumption accompanies with the rudimentally described calibration procedure by the manufacturer itself where a few calibration parameters are given [44]. Thus, the following calibration parameters are investigated corresponding to [39, 40]:

- m: scale factor, i.e., scale deviation of metrical distance measurement
- k: zero error (additive constant), i.e., the offset of distance measurement
- c: horizontal collimation error, i.e., non-orthogonality between collimation axis and trunnion axis
- i: trunnion axis error, i.e., non-orthogonality between trunnion axis and vertical axis
- h: vertical index error (vertical collimation error), i.e., deviation of vertical angle from zero at zenit
- $\varepsilon_{t,1}, \varepsilon_{t,2}$: eccentricities of horizontal graduated circle, i.e., deviation between geometrical mean of horizontal graduated circle and vertical axis
- e_y: horizontal eccentricity of collimation axis, i.e., horizontal distance between collimation axis and vertical axis
- $\varepsilon_{\beta,1}, \varepsilon_{\beta,2}$: eccentricities of vertical graduated circle, i.e., deviation between geometrical mean of vertical graduated circle and trunnion axis
- e_z: vertical eccentricity of collimation axis, i.e., vertical distance between collimation axis and trunnion axis

The most important calibration parameters are the zero error k, the horizontal collimation error c, the trunnion axis error i and the vertical index error h [4, 29]. However, the

other ones are also reasonable. A geometrical approach deriving (parts of) these errors can be found in several publications [6, 26].

3.2 Modeling systematic errors

The proposed systematic errors need to be modeled so that their impact on the raw measurements can be described. Here, a strict approach is implemented concerning the named calibration parameters. Some explanations need to be given:

- Horizontal collimation error c and trunnion axis error i impact the horizontal direction t as well as the vertical angle β. While the latter impact is usually omitted at tacheometers due to mostly horizontal observations, it is modeled here due to observations in the laser scanner's complete field-of-view. The impact is largest at low vertical angles (zenit) [43].
- The eccentricities of the horizontal and vertical graduated circles can be described by (i) the maximal angular error $\varepsilon_{\max}$ and (ii) the angle α_0 (horizontal or vertical) being affected by this maximal error the most: $\varepsilon_{\max} \cdot \sin(\alpha + \alpha_0)$. Here, $\varepsilon_{\max} = e/r$ depends on the eccentricity e and on the radius of the graduated circle r [6]. This nonlinear error model consisting of the parameters $\varepsilon_{\max}, \alpha_0$ is substituted here to a linear one consisting of $\varepsilon_{\beta,1}, \varepsilon_{\beta,2}$ or $\varepsilon_{t,1}, \varepsilon_{t,2}$, respectively, similarly to [26, 40].
- The horizontal and vertical eccentricities of the collimation axis are modeled straightforward following [6].
- The modeling of the systematic errors considers the measuring process of the Leica Scan Station P20 at a panoramic scan: the horizontal rotation only covers 200 gon by $t \in [0\ gon, 200\ gon]$ – thus, not a complete turn – and the vertical rotation covers 300 gon by $\beta \in [-150\ gon, 150\ gon]$. Consequently, points scanned by vertical angles greater than 0 gon are captured in face one, the other ones in face two.

Based on these statements, the true measurements s, β, t that suffer from unavoidable misconstruction of the TLS need to be corrected by the following equations to equal the theoretical corrected observations $\tilde{s}, \tilde{\beta}, \tilde{t}$ free of any systematic error:

$$\tilde{s}_j = m \cdot s_j + k \tag{5}$$

$$\tilde{\beta}_j = \pm \arccos\left(\cos i \cdot \cos c \cdot \cos \beta_j - \sin i \cdot \sin c\right) + h + \varepsilon_{\beta,1} \cdot \cos \beta_j + \varepsilon_{\beta,2} \cdot \sin \beta_j + \arcsin \frac{e_z}{s_j} \tag{6}$$

$$\tilde{t}_j = t_j + \arctan\left(\frac{\cos i \cdot \tan c}{\sin \beta_j} + \frac{\sin i}{\tan \beta_j}\right) + \varepsilon_{t,1} \cdot \sin t_j + \varepsilon_{t,2} \cdot \cos t_j + \arcsin \frac{e_y}{s_j} \tag{7}$$

Eq. (7) is problematic for $\beta_j = 0$ so that this value is avoided in the computation.

Considering eqs. (5–7), when parameterizing the measured point cloud of the main reflector, the object parameters $\mathbf{p}_{\text{obj}}$ need to expanded by the calibration parameters

$$\mathbf{p}_{\text{cal}} = \left[m, k, c, i, h, \varepsilon_{t,1}, \varepsilon_{t,2}, e_y, \varepsilon_{\beta,1}, \varepsilon_{\beta,2}, e_z\right]^T \tag{8}$$

that are simultaneously estimated in the complete parameter vector

$$\mathbf{p} = \begin{bmatrix} \mathbf{p}_{\text{obj}} \\ \mathbf{p}_{\text{cal}} \end{bmatrix}. \tag{9}$$

This rests upon the fact that the true observations s, β, t – suffering from the systematic errors – are integrated in eq. (1) and, thus, eqs. (2-3).

3.3 Summary of systematic errors

Due to the miscontruction of the TLS, systematic errors exist. Hence, point clouds measured by a TLS contain systematic deviations that equal the transfer of the systematic errors into the model space. These errors can be revealed if scanning an object of known shape that meets special requirements. In other words, the key to uncover the systematic deviations is the model knowledge that needs to be integrated. This is done here by parameterizing the scanned surface as a rotational paraboloid. The second requirement is a functional model parameterizing the transfer of the systematic errors to the model space. This needs to address all significant effects realistically. A common – but simplified – parameterization is the one of eqs. (5–7).

4 Simulating and analyzing the self-calibration

The main reflector of the Effelsberg radio telescope had already been scanned a few years ago for reasons of a deformation analysis. It was revealed that the focal length

Fig. 3. Station and orientation of the TLS at an elevation angle of the telescope of 90 *deg* (left) and 7.5 *deg* (right).

varies when changing the elevation angle of the telescope but that the change of the shape always resulted in a rotational paraboloid again [16, 18]. This principle is called homologous deformation.

Following, a concept for scanning the whole main reflector completely from one single station had already been built up in [18]; in the recent past, it has been optimized regarding the orientation of the TLS as will be explained in the following subsection. It rests upon scanning the main reflector in seven different elevation angles of the radio telescope where the measurement geometry between scanner and main reflector varies with the elevation angle.

The present section now aims at finding the measurement geometry being suited best for a TLS self-calibration regarding the network configuration, i.e., parameter unbiasedness, accuracies and correlation. These aspects are the most relevant ones when judging the quality of a test field for laser scanner self-calibration [28, 29].

4.1 Realization of measurements

For scanning the whole main reflector from one station, the TLS is mounted in the subreflector of the telescope so that it is upside-down at a telescope elevation of 90 *deg* (Fig. 4). From this station, the TLS scans the whole main reflector by a panoramic scan leading to approx. 500 millions of points. For better manageability, this number is reduced to approx. 400000 points using Cyclone. Furthermore, the outer 10 *m* of the main reflector cannot be used for analysis since this sector is perforated and, thus, not suited for a TLS analysis (see Fig. 1).

When tilting the telescope to a minimal elevation angle of 7.5 *deg*, this scanning geometry changes since the upside-down station of the laser scanner remains constant due to a flexible link that connects the scanner to the subreflector (Fig. 3). Seven different scans with elevation angles of 90 *deg*, 75 *deg*, 60 *deg*, 45 *deg*, 30 *deg*, 15 *deg* and 7.5 *deg* have been performed. This results in different scanning geometries when approximating the main reflector leading to several variations:

1. The main reflector cannot be scanned completely at low elevation angles (15 – 7.5 *deg*) due to the limited vertical field-of-view of the TLS of 300 *gon* (Fig. 4).
2. High vertical angles (near the laser scanner's horizon) are only measured at low elevation angles.
3. Observations in the laser scanner's zenit do not exist at low elevation angles (15 – 7.5 *deg*).

Due to this changing scanning geometry, the systematic residuals resulting from the systematic TLS errors always appear differently. It is not obvious a priori which geometry is suited best for self-calibration of the TLS. This will be analyzed in a simulation.

4.2 Parameter estimation for self-calibration

The parameters $\mathbf{p}$ (eq. 9) are estimated based on several simulations of different elevation angles of the radio telescope. Therefore, observations simulated unbiasedly are firstly manipulated following the systematic errors (eqs. 5 – 7) and afterwards randomly noised by

$$\boldsymbol{\Sigma}_{ll,j} = \begin{bmatrix} \sigma_{s,j}^2 & & \\ & \sigma_\beta^2 & \\ & & \sigma_t^2 \end{bmatrix} \tag{10}$$

where $\sigma_{s,j} = 1.0\ mm + s_j \cdot 0.02\ mm/m$, $\sigma_\beta = 2.5\ mgon$ and $\sigma_t = 2.5\ mgon$ are chosen corresponding to the manufacturer's specifications [24]. The resulting observations $\mathbf{l}_j$ are the ones that simulate the outcome of a non-calibrated TLS. A sampling density of $\Delta\beta = \Delta t = 0.7\ gon$ is chosen leading to $n \in [38000, 63000]$ sampling points for each elevation angle (Tab. 1).

These observations are approximated by the functional model of a transformed rotational paraboloid as already stated in eqs. (2–3). For estimating the parameters, the cost function $\mathbf{v}^T\boldsymbol{\Sigma}_{ll}^{-1}\mathbf{v}$ is minimized where $\mathbf{v}$ equals the vector of residuals. These residuals that are estimated iteratively in the adjustment – then called $\hat{\mathbf{v}}$ – describe the deviations between observations $\mathbf{l}$ and estimated observations $\hat{\mathbf{l}}$: $\hat{\mathbf{v}} = \mathbf{l} - \hat{\mathbf{l}}$.

This usually leads to the Gauß-Helmert model (GHM) – also known as general case of adjustment [32] – regarding

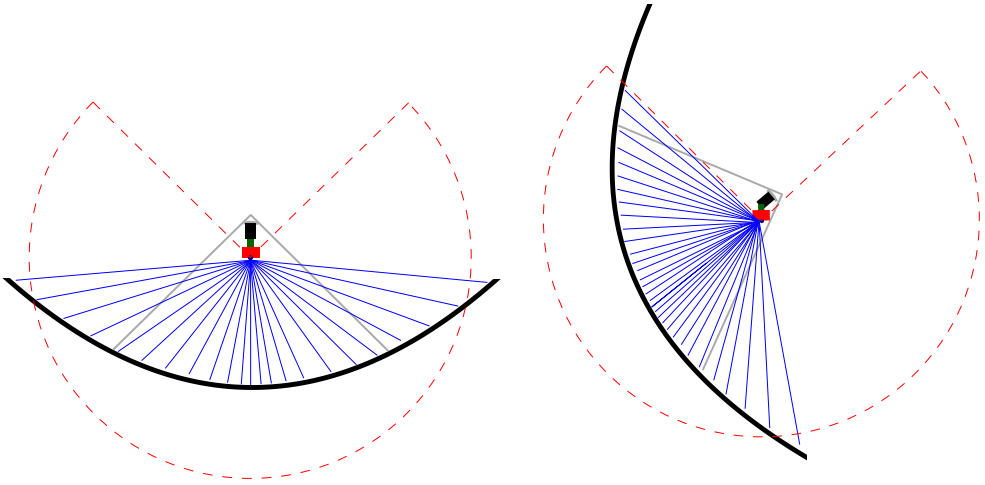

Fig. 4. Sketch of the measurement geometry, the resulting laser beam vectors (blue) inside the laser scanner's field-of-view (red dashed) and the elevation of the telescope's main reflector of 100 m diameter (black); left: 90 deg elevation, right: 30 deg elevation

the functional model. The strict solution of the nonlinear GHM is given in many publications [25, 32]; thus, it is not recapitulated here. Due to numerical reasons, the GHM is transformed to a Gauß-Markov model (GMM) leading to reduced normal equations being inverted more efficiently regarding the high number of observation at laser scanning. This transformation is similar to the one described in [17].

The results of the approximation are the estimated parameters $\hat{\mathbf{p}}$, their covariance matrix $\boldsymbol{\Sigma}_{\hat{p}\hat{p}}$ including the variances and correlations and the post-fit residuals $\hat{\mathbf{w}}$ of each sampling point, also called discrepancies in a GHM [18]. Furthermore, partial redundancies r_j are estimated. They describe the reliability of each sampling point $\mathbf{x}_j$ or observation triplet $\mathbf{l}_j$ being an indicator for the network configuration [9, 15] even when analyzing single laser scans [13, 17].

4.3 Self-calibration using all calibration parameters

At first, the self-calibration is tested by only simulating and calibrating each of the calibration parameters $\mathbf{p}_{\text{cal}}$ (eq. 8) separately. By this procedure, the general sensitivity of the network configuration regarding the specific parameter is analyzed.

As a consequence, four calibration parameters cannot be determined reliably by this network configuration – indepedent from the specific elevation angle of the telescope. These calibration parameters are the scale m, the zero error k, the horizontal eccentricity of the collimation axis e_y and one of the eccentricities of the vertical graduated circle $\varepsilon_{\beta,2}$:

- The scale m is not predictable due to the lack of reference – there is no distance that is known which would help to determine the scale. This would be different if, e.g., the focal length f of the main reflector was known.
- The zero error k is nearly correlated by 1 with the translation Z_v and the focal length f. Thus, changes in k directly lead to changes in Z_v and in f so that the residuals of the adjustment are not systematically distributed even when simulating a zero error. Simultaneously, the accuracies of the estimated parameters decrease significantly when estimating the zerror error k. These statements hold for all simulated network configurations.
- The horizontal eccentricity of the collimation axis e_y is only predictable at low elevation angles of the telescope. This is because the number of observations having a high vertical angle of $\beta > 100gon$ increases at low elevation angles. Especially the observations at the laser scanner's horizon are crucial for determining e_y. However, estimating e_y leads to extremely high correlations between all parameters independent from the actual elevation angle of the telescope. Thus, similarly to the zero error k, a simulated horizontal eccentricity of the collimation axis can completely be compensated by the other parameters. Hence, none of the network configurations is suited to estimate this calibration parameter.

– The eccentricity of the vertical graduated circle $\varepsilon_{\beta,2}$ is also not predictable due to a lack of sensitivity of the network configuration. Explanations are similar to e_y.

Therefore, using the described strategy for self-calibration suffers from the fact that the four named parameters cannot be estimated reliably. The reasons are also named so that in the discussion, it will be analyzed how to opitmize the test field for improving the network configuration regarding the predictability of these calibration parameters.

4.4 Self-calibration using a subset of calibration parameters

Now, the parameter estimation is performed with the remaining seven calibration parameters and the object parameters $\mathbf{p}_{\text{obj}}$ (eq. 4). The results are presented considering four aspects: (1) Unbiasedness of parameters, (2) parameter accuracies, (3) parameter correlation and (4) partial redundancies representing the network configuration.

(1) Unbiasedness of parameters

The parameters are all unbiased regarding their deviation from the simulated true systematic error and the corresponding standard deviation. Thus, all parameters are predictable in principle. Furthermore, the estimated residuals do not follow any systematic and are, thus, Gaußian distributed.

(2) Parameter accuracies

The parameters' standard deviations are presented in Tab. 1. As can be seen, these highly depend on the elevation angle of the telescope where two opposing systematics are revealed: the smaller the elevation angle, the worse are the estimated accuracies of the object parameters (no. 1–6). Contrary, the smaller the elevation angle, the better are the estimated accuracies of the calibration parameters (no. 7–13). These effects are the strongest at higher elevation angles. Before interpreting these results, the parameter correlations are also investigated.

(3) Parameter correlation

Fig. 5 shows the parameter correlations for the estimations at 90 *deg*, 45 *deg* and 7.5 *deg* elevation angle. Here, a high dependence on the elevation angle is also visible. Particularly interesting are the correlations between object and calibration parameters (no. 1–6 and 7–13, square top right or bottom left, respectively) and the correlations within the calibration parameters (no. 7–13, square bottom right).

The correlations between object and calibration parameters increase when decreasing the elevation angle. The ability to seperate the parameters from each other degrades. Simultaneously, the correlations within the object parameters (no. 1–6, square top left) also increase. Both aspects lead to the fact that the accuracies of the object parameters degrade with decreasing elevation angle.

The correlations within the calibration parameters develop completely oppositional. Low elevation angles lead to a decorrelation. Thus, the calibration parameters are better predictable at low elevation angles as was also shown by the parameter accuracies. This is expectable since the TLS observes points near its horizontal axis only at low elevation angles. As is long known at calibrating tacheometers, e.g., the horizontal collimation error c and the trunnion axis error i are only separatable in the horizon. This effect can be confirmed by the correlations since the ones between c and i decrease with decreasing elevation angle.

(4) Partial redundancies

Partial redundancies are already meaningful for network analyses when considering only one station and one single scan [13, 17]. Here, especially the difference in partial redundancies between estimating only the object parameters (first case) and estimating object parameters combinedly with calibration parameters (second case) is worth investigating. Fig. 6 shows both situations for an elevation angle of 45 *deg*.

The absolute values of the partial redundancies are very high in both cases and only vary little. This is typical when approximating laser scans since the number of parameters is always many times smaller than the number of observations [17]. Disregarding this fact, the variation is smaller in the first case ($\approx 3 \cdot 10^{-4}$) than in the second one ($\approx 2 \cdot 10^{-3}$). Hence, the discrepance of impact that different parts of the antenna have on the parameter estimation is higher in the second case.

While the partial redundancies are mostly due to the object geometry in the first case (the marginal parts of the antenna do have lower partial redundancies), they are mainly due to the scanning geometry in the second case: the partial redundancies only decrease symmetrically to

the laser scanner's x-axis that is projected on the telescope by a black line in Fig. 6. Thus, the systematic distribution of the partial redundancies shown in Fig. 6 rarely varies between the different elevation angles in the first case, while it varies completely in the second case.

Consequently, while the scanning geometry does not seem to be the crucial aspect for parameter estimation when considering only object parameters, it is when estimating also the calibration parameters. This explains the high dependence of the calibration approach on the scanning geometry and, hence, on the elevation angle of the telescope. The significance of this effect is, furthermore, enlarged by the fact that the magnitude of variation of the partial redundancies is increased when estimating also the calibration parameters.

4.5 Reduction of sampling points

The previous subsection has shown that the calibration parameters can indeed be estimated. The estimated parameters are always unbiased regarding their standard deviation. Since this standard deviation correlates with the number of sampling points, this number is reduced now. This shall highglight the signficance of an appropriate stochastic model for this analysis.

Following, the sampling density of vertical and horizontal angles is reduced to $\Delta\beta = \Delta t = 10\ gon$ leading to $n \in [310, 187]$ sampling points for each elevation angle. The subsequent approximation leads to the standard deviations printed in Tab. 2 where the corresponding parameters are again estimated unbiasedly.

The standard deviations are – as expected – proportionally degraded following the $\sqrt{n}$-law. This results in magnitudes of the standard deviations being in a range where the estimation is hardly feasible since, e.g., a horizontal collimation error c needs to be larger than 20 $mgon$ to be significantly estimated at an elevation angle of 60 deg. Hence, the number of points is the relevant aspect for attesting the predictability of the calibration parameters.

Clearly, assuming a laser scan to consist of only about 300 points is unrealistic. But assuming a laser scan to consist of, e.g., 500000 points that are all uncorrelated is similarly unrealistic. Correlations are definitely existent when scanning a surface due to similar angles of impact, reflectivity, atmospherical conditions, insufficient modeled systematic errors, etc.

Consequently, for interpreting the results, a realistic stochastic model is necessary that does not imply large significance of the estimated parameters by neglecting correlations. In practice, the accuracy of the estimated parameters does not improve by the $\sqrt{n}$-law due to these neglected correlations. Here, the effective number of measurements should be estimated that determines the true number of independent observations [22]. This would be – similarly to, e.g., GPS observations [23] – many times smaller than the number of observations.

4.6 Summary of simulation

The results of this simulation show that some of the calibration parameters, i.e., m, k, e_y, $\varepsilon_{\beta,2}$, are generally not predictable using the presented approach. Furthermore, the elevation angle of the telescope determining the scanning geometry is essential for a reliable self-calibration of the TLS. Here, the quality of the parameters (accuracy, correlation) diverges between object parameters and calibration parameters when changing the elevation angle of the telescope. For calibrating the TLS, an elevation angle of 30 deg or 45 deg seems to be best when studying the standard deviations and correlations of the calibration parameters (Tab. 1 and Fig. 5). The ones of the object parameters are irrelevant for calibration.

Regarding these standard deviations, the simulation of fewer sampling points strongly insists that the quality of the estimation is governed by the number of uncorrelated points and a realistic stochastic model. Thus, the presented strategy for self-calibration does not benefit from an advantageously network configuration for estimating the calibration parameters but from the large number of observations. Actually, the network configuration is rather weak concerning the calibration parameters.

5 Results of self-calibration

The previous section insists calibrating the TLS at an elevation angle of 30 deg or 45 deg. Thus, the calibration parameters will be estimated in the following based on the real scans at these elevation angles. An analysis of their magnitude and variation and the assessment of the postfit residuals leads to an evaluation.

5.1 Analysis of calibration parameters

Following the previous statements, the TLS is self-calibrated. This leads to the calibration parameters and corresponding standard deviations presented in Tab. 3 where the number of points equals $n = 408067$ at 45 deg

Table 1. Estimated standard deviations of the object parameters and calibration parameters as a result of the simulation corresponding to different elevation angles of the radio telescope; simulated angular increments: $\Delta\beta = \Delta t = 0.7\ gon$ leading to n sampling points.

No.	Parameter	*90 deg*	*75 deg*	*60 deg*	*45 deg*	*30 deg*	*15 deg*	*7.5 deg*
	n	62874	62564	61603	59605	55208	42206	38278
1	$X_v\ [mm]$	0.31	0.31	0.31	0.32	0.38	0.64	0.86
2	$Y_v\ [mm]$	0.72	0.66	0.58	0.58	0.67	0.75	0.74
3	$Z_v\ [mm]$	0.01	0.02	0.02	0.02	0.02	0.02	0.03
4	$\varphi_x\ [mgon]$	1.27	1.27	1.36	1.72	2.71	5.22	8.15
5	$\varphi_y\ [mgon]$	0.52	0.52	0.52	0.53	0.68	1.35	1.89
6	$f\ [mm]$	0.11	0.12	0.13	0.13	0.14	0.18	0.22
7	$c\ [mgon]$	4.18	0.96	0.56	0.40	0.32	0.32	0.37
8	$i\ [mgon]$	5.16	1.23	0.71	0.45	0.31	0.25	0.27
9	$h\ [mgon]$	2.31	0.72	0.61	0.59	0.60	0.65	0.71
10	$\varepsilon_{t,1}\ [mgon]$	7.58	1.57	0.88	0.67	0.65	0.84	0.98
11	$\varepsilon_{t,2}\ [mgon]$	7.38	0.87	0.51	0.44	0.41	0.46	0.52
12	$\varepsilon_{\beta,1}\ [mgon]$	2.39	0.34	0.15	0.12	0.12	0.16	0.19
13	$e_z\ [mm]$	2.08	0.45	0.34	0.32	0.33	0.37	0.39

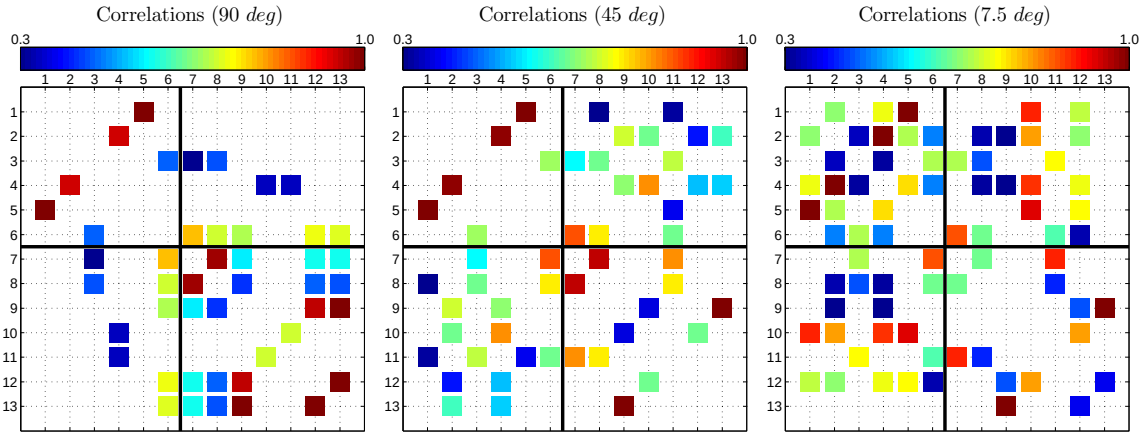

Fig. 5. Correlations between the estimated parameters $\hat{\mathbf{p}}$ at different elevation angles of the radio telescope; 1: X_v, 2: Y_v, 3: Z_v, 4: φ_x, 5: φ_y, 6: f, 7: c, 8: i, 9: h, 10: $\varepsilon_{t,1}$, 11: $\varepsilon_{t,2}$, 12: $\varepsilon_{\beta,1}$, 13: e_z; correlations minor 0.3 are not shown.

Table 2. Estimated standard deviations of the object parameters and calibration parameters as a result of the simulation corresponding to different elevation angles of the radio telescope; simulated angular increments: $\Delta\beta = \Delta t = 10\ gon$ leading to n sampling points.

No.	*Parameter*	*90 deg*	*75 deg*	*60 deg*	*45 deg*	*30 deg*	*15 deg*	*7.5 deg*
	n	310	308	297	294	269	207	187
1	$X_v\ [mm]$	4.58	4.35	4.69	4.37	5.28	8.49	11.75
2	$Y_v\ [mm]$	9.89	9.27	8.83	7.84	10.03	10.10	10.31
3	$Z_v\ [mm]$	0.16	0.25	0.33	0.31	0.30	0.33	0.37
4	$\varphi_x\ [mgon]$	17.54	17.88	20.70	23.11	40.47	68.65	111.71
5	$\varphi_y\ [mgon]$	7.60	7.19	7.88	7.11	9.35	17.58	25.35
6	$f\ [mm]$	1.44	1.71	2.00	1.78	2.12	2.44	3.16
7	$c\ [mgon]$	54.04	13.43	8.62	5.33	4.52	4.49	5.32
8	$i\ [mgon]$	67.36	17.38	10.68	6.14	4.44	3.40	3.83
9	$h\ [mgon]$	33.46	9.86	9.42	7.77	9.08	9.06	10.16
10	$\varepsilon_{t,1}\ [mgon]$	95.14	22.78	12.99	9.06	9.39	10.78	12.86
11	$\varepsilon_{t,2}\ [mgon]$	113.61	11.71	7.67	5.93	5.36	6.12	7.10
12	$\varepsilon_{\beta,1}\ [mgon]$	35.12	4.73	2.24	1.67	1.95	2.03	2.50
13	$e_z\ [mm]$	30.31	6.15	5.11	4.24	4.86	5.14	5.69

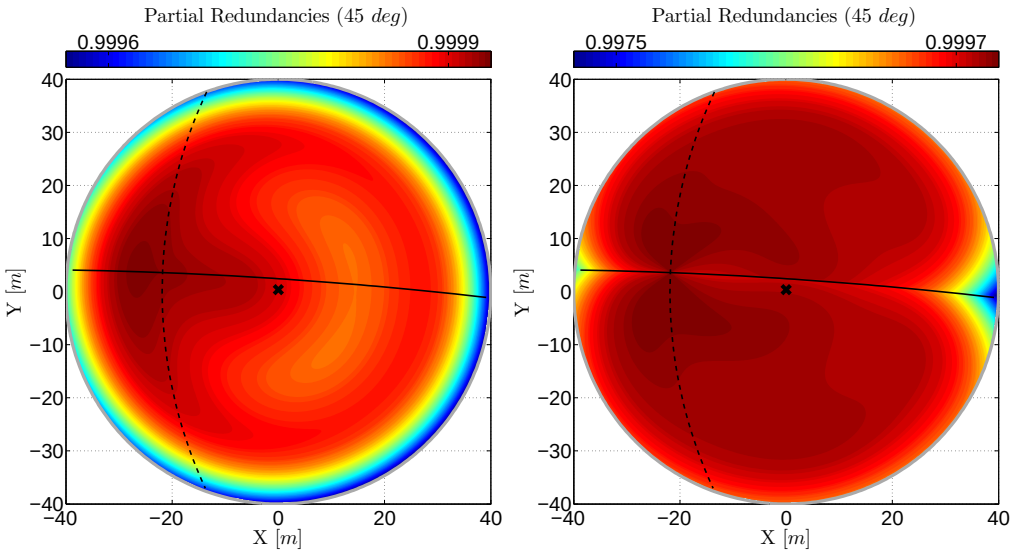

Fig. 6. Partial redundancies of the sampling points at an elevation angle of 45 *deg* shown in object coordinate system $[X, Y, Z]$; transformation of TLS x-axis (lined), y-axis (dashed) and station (cross) in object coordinate system; left: estimating only the object parameters; right: estimating object as well as calibration parameters.

elevation angle and $n = 398543$ at 30 *deg*. Simultaneously, the parameters are estimated after reducing the sampling points to a grid of approx. 2.5 *m* point distance leading to the results of Tab. 4. The number of points reduces to $n = 606$ (45 *deg*) and $n = 586$ (30 *deg*). Comparing both tables (different number of sampling points) and also the different values within each table (different elevation angle for estimation), large deviations are revealed.

After all, the tables insist that the calibration parameters are not physically interpretable: they vary extremely between 45 *deg* and 30 *deg* elevation angle and their significance is only given if a large number of observations is used for estimation. Furthermore, they vary when reducing the data. Hence, no statement regarding the magnitude and the significance of the calibration parameters is possible.

This situation is due to two reasons: (1) the functional model is insufficient and (2) the stochastic model neglects correlations. The first reason bases upon the assumed calibration parameters and their functional model (eqs. 5–7) building the transformation into model space. This model is only an approximation that is – due to the resctrictive announcement of the manufacturers – incorrect. Additionally, not all parameters of this simplified model that have been introduced in Section 3 are predictable. Thus, if the corresponding error sources (or similar ones) are present, they can have a different impact on the estimation results that depends on the elevation. Hence, the calibration parameters vary and are not physically interpretable.

Additionally, this situation and other effects lead to correlations that are also not modeled in the adjustment so that an assessment of the true level of accuracy of the estimated parameters is hardly feasible. It is simply not possible to determine the magnitude at which parameters deviate significantly since the estimated standard deviations are too optimistic.

5.2 Analysis of post-fit residuals

Disregarding the limitations formulated in the previous subsection, the systematic deviations in the residuals can be eliminated by simultaneously estimating the calibration parameters and the object parameters. This is shown in Fig. 7 for an elevation angle of 45 *deg* where the original residuals – without calibration – are opposed to the ones resulting after calibration. The remaining noise is Gaußian distributed. The apparent systematic deviations visible at a few positions on the main reflector should not bother this result since these can be related to real deformations on the main reflector [14].

Furthermore, the residuals after calibration have a standard deviation of about $\hat{\sigma}_w = 1.3$ *mm*. This value approximately agrees with the assumed standard deviation of the distance unit of $\sigma_s = [1.6, 1.8]$ *mm* at distances between 30 – 40 *m*. Thus, this approximation is successful and the calibration works considering this single scan. The same applies if using the results of the elevation angle 30 *deg*.

Table 3. Estimated calibration parameters at elevation angles of 45 *deg* (n = 408067 sampling points) and 30 *deg* (n = 398543).

elev.	*value*	*c [mgon]*	*i [mgon]*	*h [mgon]*	$\varepsilon_{t,1}$ *[mgon]*	$\varepsilon_{t,2}$ *[mgon]*	$\varepsilon_{\beta,1}$ *[mgon]*	e_z *[mm]*
45 *deg*	parameter	0.41	17.29	1.45	2.62	-6.62	2.46	-1.92
	std. dev.	0.16	0.18	0.27	0.22	0.19	0.05	0.15
30 *deg*	parameter	0.40	35.71	-12.53	-0.05	-12.42	1.66	2.27
	std. dev.	0.17	0.12	0.32	0.24	0.20	0.06	0.18

Table 4. Estimated calibration parameters at elevation angles of 45 *deg* (n = 606 sampling points) and 30 *deg* (n = 586) using downsampled point clouds.

elev.	*value*	*c [mgon]*	*i [mgon]*	*h [mgon]*	$\varepsilon_{t,1}$ *[mgon]*	$\varepsilon_{t,2}$ *[mgon]*	$\varepsilon_{\beta,1}$ *[mgon]*	e_z *[mm]*
45 *deg*	parameter	-2.36	19.82	1.91	4.04	-4.41	1.76	-1.80
	std. dev.	3.68	4.34	6.37	5.56	4.45	1.04	3.75
30 *deg*	parameter	0.24	36.57	-12.98	-0.42	-10.06	0.81	2.35
	std. dev.	3.72	2.84	7.24	5.77	4.78	1.32	4.18

5.3 Calibration of all laser scans

The previously estimated calibration parameters – using elevation angles of 45 *deg* and 30 *deg* – are used to calibrate all laser scanner measurements. Afterwards, the object parameters are estimated without additionally estimating the calibration parameters. Fig. 8 exemplarily shows the post-fit residuals of the approximation at an elevation angle of 75 *deg* when using the calibration parameters estimated at 45 *deg* elevation angle. These can be compared to the original ones of Fig. 2. Clearly, the calibration improved the results.

To compare the results of all scans before and after calibration (by either using the parameters of 45 *deg* elevation angle or 30 *deg*), the estimated standard deviations $\hat{\sigma}_w$ of the post-fit residuals $\hat{\mathbf{w}}$ are calculated and presented in Tab. 5. As can be seen, the improvement is not the same at each elevation angle. In fact, it is also different between using the 45 *deg* scan or the 30 *deg* scan for calibration. This result is expectable based on the large variations of the calibration parameters estimated at different elevation angles (Tab. 3).

5.4 Dynamic calibration

For discussion, the standard deviations of the post-fit residuals when estimating calibration parameters at each elevation angle separately are also listed in Tab. 5. They are significantly smaller than in the original calibration. Their magnitude approx. equals 1.3 *mm* each time. This magnitude seems to represent the true noise of the TLS distance measurements since the post-fit residuals approximately point in line-of-sight of the scanner.

However, the calibration parameters are estimated seven times in this scenario leading to a significant variation as has already been seen in Tab. 3 for 45 *deg* and 30 *deg* elevation angle. Hence, this procedure – named dynamic calibration from now on – works, but contradicts the idea of determining constant calibration parameters for a TLS.

5.5 Summary of calibration

Even though calibration parameters are predictable following the previous simulation, the values estimated by the real scans are not meaningful. This is due to an insufficient functional and stochastic model. This functional model transfering the systematic TLS erorrs to the model space needs to be more realistic as well as the assessment of correlations and variances needs to be improved. Both aspects affect the calibration parameters significantly since the network configuration is rather weak. The strong advantage of this approach – the large number of observations used for calibration – can only be effectively used with improved functional and stochastic model.

Nevertheless, the systematic deviations resulting from the TLS errors can be eliminated by estimating the calibration parameters at each scan separately. This procedure is suited to reduce the systematic deviations in the point cloud and, thus, to improve the surface analysis. However, it does not represent the primary idea of a self-calibration estimating one set of physically interpretable parameters being constant over time. Instead, it is rather a data-fit.

Table 5. Estimated standard deviation $\hat{\sigma}_w$ of the post-fit residuals $\hat{\mathbf{w}}$ before and after calibration of the measurements based on n sampling points.

value	*90 deg*	*75 deg*	*60 deg*	*45 deg*	*30 deg*	*15 deg*	*7.5 deg*
n	376139	382615	396074	408067	398543	379487	359791
$\hat{\sigma}_w$ $[mm]$ (without calibration)	1.45	1.60	1.56	1.47	2.05	1.88	1.83
$\hat{\sigma}_w$ $[mm]$ (calibration by 45 deg)	1.46	1.42	1.36	1.27	1.63	1.53	1.49
$\hat{\sigma}_w$ $[mm]$ (calibration by 30 deg)	2.01	1.98	1.45	1.58	1.29	1.44	1.48
$\hat{\sigma}_w$ $[mm]$ (dynamic calibration)	1.35	1.32	1.28	1.27	1.29	1.31	1.30

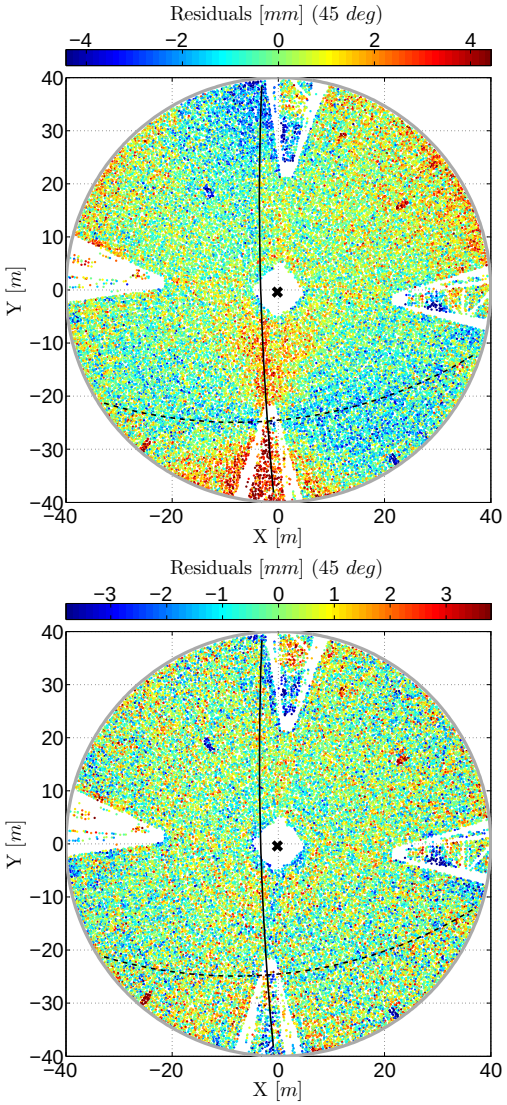

Fig. 7. Post-fit residuals of the approximation at an elevation angle of 45 deg shown in object coordinate system $[X, Y, Z]$; transformation of TLS x-axis (lined), y-axis (dashed) and station (cross) in object coordinate system; top: before calibration; bottom: after calibration.

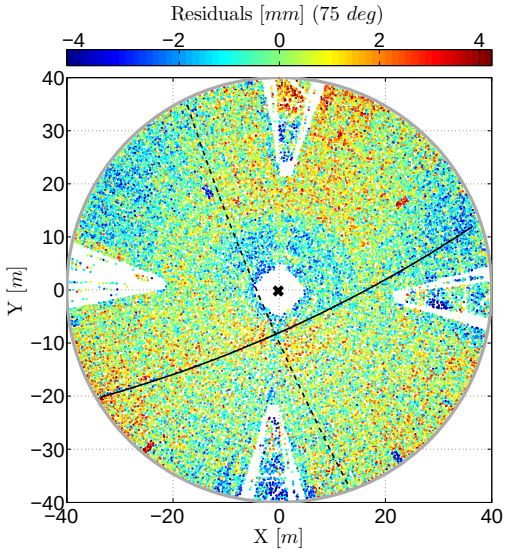

Fig. 8. Post-fit residuals of the approximation at an elevation angle of 75 deg after calibration shown in object coordinate system $[X, Y, Z]$; transformation of TLS x-axis (lined), y-axis (dashed) and station (cross) in object coordinate system.

6 Discussion

Previous calibration strategies use the parameter differences of a limited number of objects scanned from different stations for estimating the calibration parameters. While it is not satisfactory in this approach that the large number of observations is reduced to a limited number of objects, it benefits from a strong network configuration.

The present study investigates a new approach for TLS self-calibration. The idea is to use all deviations between the best-fit surface of a scanned object and the point cloud to estimate the calibration parameters. This enables a calibration by one single scan of one single object. This procedure benefits from the large number of observations and each point's individual information about the systematic TLS errors. But simultaneously, it suffers from the weak configuration of adjustment that is due to the sampled object and the scanning geometry.

The results of the simulation show that the new approach is principially suited for estimating calibration parameters. Thus, systematic TLS errors can be separated from the scanned object. Anyhow, the calibration parameters vary significantly at the real calibration of the Leica Scan Station P20 using this approach. Thus, the approximation upgrades only partially when using one set of calibration parameters.

Nevertheless, when estimating the calibration parameters separately for each scan, the post-fit residuals are improved leading to purely Gaußian distributed noise. This distribution contains a standard deviation of approximately 1.3 mm at each elevation angle. This magnitude can be assumed to represent the true random noise of the distance unit of the TLS – which is of expected magnitude. Consequently, from the view of adjustment, the approximation is successful. However, the calibration parameters are not constant in this procedure and, hence, not physically interpretable. This approach that can be seen as a pure data-fit is called dynamic calibration here.

Not being able to estimate constant and physical interpretable calibration parameters – at this time – is due to several reasons. These are based either on (1) the functional model parameterizing the systematic TLS erorrs, (2) the corresponding stochastic model, (3) the scanned object for self-calibration that is presented here and (4) the scanning geometry.

(1) Functional model parameterizing the systematic errors

For parameterizing the systematic TLS errors, standard parameters corresponding to a tacheometer are considered. This assumption is only approximative and does not reflect the reality since the beam deflection even of a panoramic TLS differs from the one of a tacheometer. While it seems to be evident that a TLS also suffers from systematic errors like a horizontal collimation error or a trunnion axis error, it is not obvious how these errors affect the measured angles. This could be totally different from the assumption in eqs. (5–7) which is also addressed in [12, 33].

Thus, the model for parameterizing the systematic errors of the TLS including the types of errors needs to be improved. Therefore, the true course of the laser beam inside the TLS and the possible misconstructions leading to systematic errors should be reproduced better.

(2) Stochastic model

The ability of estimating the calibration parameters does not rest upon a sophisticated and detailedly planned network configuration but on the large number of observations. As has been shown, this large number causes the standard deviations of the calibration parameters to be small regarding the calibration parameters' expected magnitude. However, a qualified assessment of the estimated calibration parameters is only approvable if the stochastic model reflects the reality sufficiently.

This has to be classified critically if it does not consider correlations so that each individual point is assumed to contain completely independent information. These correlations are contained in TLS measurements in any case due to, e.g., similar angle of incidences, reflectations, unmodeled systematic errors. Hence, the quality of the calibration parameters is overestimated and significance is assumed that does probably not exist.

(3) Scanned object

Using the main reflector of a radio telescope for self-calibration is feasible. The calibration process benefits from the large size, the precise construction and the simple form that can be parameterized by the focal length. This object nearly covers the complete panoramic scan in horizontal as well as in vertical deflection, the measured distances range between 30 – 40 m.

Apart from these advantages, one drawback remains: not knowing the focal length of the main reflector – whose estimation is the aim of a separate deformation analysis – leads to the fact that some calibration parameters are worse predictable or even not predictable at all. E.g., the scale would be predictable if the focal length was known.

Thus, further model knowledge of the scanned object would upgrade the self-calibration. Simulations show that the correlations of the calibration parameters would decrease if the focal length was known. Contrary, the standard deviations of the calibration parametes would only benefit partially.

(4) Scanning geometry

The scanning geometry is a crucial aspect since it determines – mainly together with the object geometry – the network configuration of the adjustment. Contrary to the known calibration fields, this network configuration can-

not be optimized by a sophisticated arrangement of signalized targets or planes.

Consequently, the scanning geometry can only be arranged by the station of the TLS (if the object is already given). The used station leads to a nearly perfect sampling of the whole main reflector – however, it leads to high correlations of the calibration parameters. Thus, an estimation is only reliably and accurately feasible at some elevation angles; 45 – 30 *deg* seem to be the best choice.

Scanning points near the scanner's horizontal axes is crucial for determining the calibration parameters as has been shown. Thus, horizontal observations in all scans would upgrade the calibration procedure and the ability to use the scan at 90 *deg* elevation for self-calibration. This would be possible if the radio telescope was either larger in diameter (with the same focal length) or had a shorter focal length (with the same diameter). On the other hand, the scanner could be stationed closer to the main reflector for producing horizontal observations.

7 Conclusion and outlook

The present study investigates a new concept for laser scanner self-calibration. Referring to the introduction, the following questions are to answer: is it feasible to self-calibrate a TLS based upon one single scan of one single object? If yes, which requirements have to be met regarding (1) the scanned object, (2) the measurement geometry, (3) functional model of the calibration parameters and (4) stochastic model of the adjustment? After the simulation and the processing of real data, the answer is split:

- Yes, a self-calibration using one single scan of one single object is feasible in principle. This is based on the integration of model knowledge, i.e., the parameterization of the scanned object as a rotational paraboloid.
- No, a self-calibration using one single scan of one single object is not feasible at the moment since great demands on the aspects (1–4) are made that cannot be fulfilled yet.

This altogether rests upon the fact that the network configuration is rather weak regarding the sensitivity for predicting the calibration parameters. This can only be compensated by the large number of observations if aspects (1–4) are built up appropriately. To gain physically interpretable calibration parameters, especially the functional and stochastic model need to be upgraded further.

After all, this study aims at directing further research since the presented strategy's main advantage is beyond controversy: each measured point – including its individual information about the systematic TLS errors – is used directly for estimating the calibration parameters. By improving the functional and stochastic model for calibration, the potential of the presented approach will be investigated further in consecutive studies.

References

[1] Abbas M. A., Setan H., Majid Z., Idris K. M., Mohd Ariff M. F., Chong A. K. and Lichti D. D., The effect of datum constraints for terrestrial laser scanner self-calibration, in: *FIG Congress 2014, Kuala Lumpur, Malaysia 16-21 June 2014*, 2014.

[2] Bae K. -H. and Lichti D. D., On-site self-calibration using planar features for terrestrial laser scanners, in: *ISPRS Workshop on Laser Scanning 2007 and SilviLaser 2007, Espoo, September 12-14, 2007, Finland*, 2007.

[3] Chow J. C. K., Lichti D. D. and Glennie C., Point-based versus plane-based self-calibration of static terrestrial laser scanners, *Int. Arch. Photogramm. Remote Sens. Spat. Inf. Sci.* 38 (2011).

[4] Chow J. C. K., Lichti D. D., Glennie C. and Hartzell P., Improvements to and comparison of static terrestrial lidar selfcalibrationa methods, *Sensors* 13 (2013), 7224–7249.

[5] Chow J. C. K., Lichti D. D. and Teskey W., Accuracy assessment of the Faro Focus3D and Leica HDS6100 panoramic type terrestrial laser scanner through point-based and plane-based user self-calibration, in: *Proceedings of the FIG Working Week: Knowing to Manage the Territory, Protect the Environment, Evaluate the Cultural Heritage, Rome, Italy (2012)*: 6-10., 2012.

[6] Deumlich F. and Staiger R., *Instrumentenkunder der Vermessungstechnik*, 9 ed, Wichmann, Heidelberg, 2002.

[7] Dorninger P., Nothegger C., Pfeifer N. and Molnár G., On-thejob detection and correction of systematic cyclic distance measurement errors of terrestrial laser scanners, *J. Appl. Geodesy* 2 (2008), 191–204.

[8] Eling D., *Terrestrisches Laserscanning für die Bauwerksüberwachung*, Ph.D. thesis, Wissenschaftliche Arbeiten der Fachrichtung Geodäsie und Geoinformatik der Leibniz Universität Hannover, no. 282, 2009.

[9] Förstner W., Reliability analysis of parameter estimation in linear models with applications to mensuration problems in computer vision, *Comput. Vision. Graph.* 40 (1987), 273–310.

[10] García-San-Miguel D. and Lerma J. L., Geometric calibration of a terrestrial laser scanner with local additional parameters: An automatic strategy, *ISPRS J. Photogramm. 79* (2013), 122–136.

[11] Gielsdorf F., Rietdorf A. and Gründig L., A concept for the calibration of terrestrial laser scanners, in: *FIG Working Week 2004, Athens, Greece, May 22-27, 2004*, 2004.

[12] Gordon B., *Zur Bestimmung von Messunsicherheiten terrestrischer Laserscanner*, Ph.D. thesis, Fachbereich Bauingenieurwesen und Geodäsie der Technischen Universität Darmstadt, D 17, 2008

[13] Holst C., Artz T. and Kuhlmann H., Biased and unbiased estimates based on laser scans of surfaces with unknown deforma-

tions, *J. Appl. Geodesy* 8 (2014), 169–184.
[14] Holst C., Dupuis J., Paulus S. and Kuhlmann H., Flächenhafte Deformationsanalysen mit terrestrischen und Nahbereichslaserscannern - eine Gegenüberstellung anhand von Beispielen, *Allgem. Verm. Nachr.* 7 (2014).
[15] Holst C., Eling C. and Kuhlmann H., Automatic optimization of height network configurations for detection of surface deformations, *J. Appl. Geodesy* 7 (2013), 103–113.
[16] Holst C. and Kuhlmann H., Bestimmung der elevationsabhängigen Deformation des Hauptreflektors des 100mRadioteleskops Effelsberg mit Hilfe von Laserscannermessungen, in: *Schriftenreihe DVW, Band 66: Terrestrisches Laserscanning - TLS 2011 mit TLS-Challenge, Wißner*, pp. 161–180, Augsburg, 2011.
[17] Holst C. and Kuhlmann H., *Impact of spatial point distributions at laser scanning on the approximation of deformed surfaces*, Ingenieurvermessung 14. Beiträge zum 17. Internationalen Ingenieurvermessungskurs, A. Wieser, Zurich, 2014, pp. 269–282.
[18] Holst C., Zeimetz P., Nothnagel A., Schauerte W. and Kuhlmann H., Estimation of focal length variations of a 100-m radio telescope's main reflector by laser scanner measurements, *J. Surv. Eng.* 138 (2012), 126–135.
[19] Kaasalainen S., Krooks A., Kukko A. and Kaartinen H., Radiometric calibration of terrestrial laser scanners with external reference targets, *Remote Sens.* 1 (2009), 144–158.
[20] F. Kern, Prüfen und Kalibrieren von terrestrischen Laserscannern, in: *Photogrammetrie, Laserscanning, Optische 3DMesstechnik. Heidelberg: Wichmann*, 2008.
[21] Kern F. and Huxhagen U., Ansätze zur systematischen Kalibrierung und Prüfung von terrestrischen Laserscannern (TLS), in: Terrestrisches Laserscanning (2008), Schriftenreihe des DVW, Band 54, Wissner, pp. 111–124, Augsburg, 2008.
[22] Kuhlmann H., Importance of autocorrelation for parameter estimation in regression models, in: *Proceedings 10th FIG International Symposium on Deformation Measurements*, pp. 354–361, 2001.
[23] Kuhlmann H., Kalman-filtering with coloured measurement noise for deformation analysis, in: *Proceedings, 11th FIG Symposium on Deformation Measurements, Santorini, Greece*, 2003.
[24] Leica Geosystems, *Leica ScanStation P20, industry's best performing ultra-high speed scanner*, www.leica-geosystems.de, 30.07.2014.
[25] Lenzmann L. and Lenzmann E., Strenge Auswertung des nichtlinearen Gauß-Helmert-Modells, *Allgem. Verm. Nachr.* 2 (2003), 68–73.
[26] Lichti D. D., Error modelling, calibration and analysis of an AMCW terrestrial laser scanner system, *ISPRS J. Photogramm.* 61 (2007), 307–324.
[27] Lichti D. D., The impact of angle parameterisation on terrestrial laser scanner self-calibration, *Int. Arch. Photogramm. Remote Sens. Spat. Inf. Sci.* 38 (2009), 171–176.
[28] D.D. Lichti, Terrestrial laser scanner self-calibration: Correlation sources and their mitigation, ISPRS J. Photogramm. 65 (2010), 93–102.
[29] Lichti D. D., Chow J. and Lahamy H., Parameter de-correlation and model-identification in hybrid-style terrestrial laser scanner self-calibration, *ISPRS J. Photogramm.* 66 (2011), 317–326.
[30] Lichti D. D. and Licht M. G., Experiences with terrestrial laser scanner modelling and accuracy assessment, in: *Int. Arch. Photogramm. Remote Sens. Spat. Inf. Sci.*, 36, pp. 155–160, 2006.
[31] Linstaedt M., Kersten T., Mechelke K. and Graeger T., *Prüfverfahren für terrestrische Laserscanner - Gemeinsame geometrische Genauigkeitsuntersuchungen verschiedener Laserscanner an der HCU Hamburg*, Photogrammetrie, Laserscanning, Optische 3D-Messtechnik - Beiträge der Oldenburger 3D-Tage 2012, Th. Luhmann / Ch. Müller, Wichmann, VDE Verlag GmbH, Berlin, Offenbach, 2012, pp. 264–275.
[32] Mikhail E. M. and Ackermann F., *Observations and least squares*, Dun-Donelly, New York, 1976.
[33] European Patent Office, EP 2 523 017 A1: *Kalibrierverfahren für ein Gerät mit Scanfunktionalität*, 2012.
[34] Paulus S., Dupuis J., Mahlein A-K. and Kuhlmann H., Surface feature based classification of plant organs from 3D laserscanned point clouds for plant phenotyping, *BMC Bioinformatics* 13 (2013), 238.
[35] Reshetyuk Y., Calibration of terrestrial laser scanners Callidus 1.1, Leica HDS 3000 and Leica HDS 2500, *Survey Review* 38 (2006), 703–713.
[36] Reshetyuk Y., *Self-calibration and direct georeferencing in terrestrial laser scanning*, Ph.D. thesis, KTH - Royal Institute of Technology, 2009.
[37] Reshetyuk Y., A unified approach to self-calibration of terrestrial laser scanners., *ISPRS J. Photogramm.* 65 (2010), 445– 456.
[38] Rietdorf A., *Automatisierte Auswertung und Kalibrierung von scannenden Messsystemen mit tachymetrischem Messprinzip*, Ph.D. thesis, DGK, 582, 2005.
[39] Schneider D., Calibration of a Riegl LMS-Z420i based on a multi-station adjustment and a geometric model with additional parameters, *Int. Arch. Photogramm. Remote Sens. Spat. Inf* 38 (2009), 177–182.
[40] Schneider D. and Schwalbe E., Integrated processing of terrestrial laser scanner data and fisheye-camera image data, *Int. Arch. Photogramm. Remote Sens. Spat. Inf. Sci.* 37 (2008).
[41] Schulz T., *Calibration of a Terrestrial Laser Scanner for Engineering Geodesy*, Ph.D. thesis, ETH Zürich, 2007.
[42] Soudarissanane S., Lindenbergh R., Menenti M. and Teunissen P., Scanning geometry: influencing factor on the quality of terrestrial laser scanning points, *ISPRS J. Photogramm.* 66 (2011), 389–399.
[43] Stahlberg C., Eine vektorielle Darstellung des Einflusses von Ziel- und Kippachsenfehler auf die Winkelmessung, *zfv* 5 (1997), 225–235.
[44] Tuexsen H. -H., Factory calibration and field verification of Leica scanners, *Geomatics World* March / April (2014), 22–25.
[45] Tuexsen H. -H., *personal communication*, Leica Geosystems, July 2014.
[46] Wang J., *Towards deformation monitoring with terrestrial laser scanning based on external calibration and feature matching methods*, Ph.D. thesis, Wissenschaftliche Arbeiten der Fachrichtung Geodäsie und Geoinformatik der Leibniz Universität Hannover, no. 308, 2013.
[47] Wunderlich T., Wasmeier P., Ohlmann-Lauber J., Schäfer T. and Reidl F., *Objektivierung von Spezifikationen Terrestrischer Laserscanner - Ein Beitrag des Geodätischen Prüflabors der Technischen Universtität München*, Blaue Reihe des Lehrstuls für Geodäsie, Heft 20, 02/2013, TU München, Germany, 2013